

## Hydrostatic Pressure Effect on Micro Air Bubbles Deposited on Surfaces with a Retreating Tip

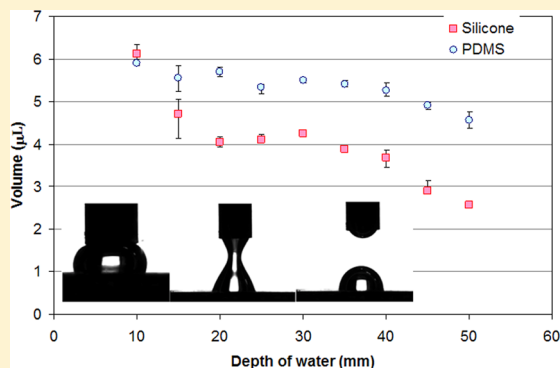
So Hung Huynh,<sup>†</sup> Jingming Wang,<sup>‡</sup> Yang Yu,<sup>§</sup> and Tuck Wah Ng\*,<sup>†</sup>

<sup>†</sup>Laboratory for Optics and Applied Mechanics, Department of Mechanical & Aerospace Engineering, Monash University, Clayton, Victoria 3800, Australia

<sup>‡</sup>School of Chemistry and Environment, Beihang University, Beijing 100191, China

<sup>§</sup>Biomechanics and Biomaterials Laboratory, Department of Mechanics, School of Aerospace Engineering, Beijing Institute of Technology, Beijing 100081, China

**ABSTRACT:** The effect of hydrostatic pressure on 6  $\mu\text{L}$  air bubbles formed on micropillar structured PDMS and silicone surfaces using a 2 mm diameter stainless steel tip retracted at 1 mm/s was investigated. Dimensional analysis of the tip retraction process showed the experiments to be conducted in the condition where fluid inertial forces are comparable in magnitude with surface tension forces, while viscous forces were lower. Larger bubbles could be left behind on the structured PDMS surface. For hydrostatic pressures in excess of 20 mm  $\text{H}_2\text{O}$  (196 Pa), the volume of bubble deposited was found to decrease progressively with pressure increase. The differences in width of the deposited bubbles (in contact with the substrate) were significant at any particular pressure but marginal in height. The attainable height before rupture reduced with pressure increase, thereby accounting for the reducing dispensed volume characteristic. On structured PDMS, the gaseous bridge width (in contact with the substrate) was invariant with tip retraction, while on silicone it was initially reducing before becoming invariant in the lead up to rupture. With silicone, hence, reductions in the contact width and height were both responsible for reduced volumes with pressure increase. Increased hydrostatic pressure was also found to restrict the growth in contact width on silicone during the stage when air was injected in through the tip. The ability to effect bubble size in such a simple manner may already be harnessed in nature and suggests possibilities in technological applications.



### INTRODUCTION

Unlike liquid drops in air subject to gravity, gas bubbles can form and float freely for an extended period in liquid bodies from processes such as priming or cavitation. They have been harnessed for applications such as enhancing heat and mass transfer,<sup>1</sup> propulsion,<sup>2</sup> providing a platform for biochemical synthesis,<sup>3</sup> enhancing cell lysis,<sup>4</sup> drug delivery,<sup>5</sup> improving contrast in ultrasonic imaging,<sup>6</sup> and enhancing or reducing the attachment of liquid drops on surfaces.<sup>7,8</sup> In some cases, however, bubbles are a nuisance. They clog microfluidic channels<sup>9</sup> and deteriorate the performance of microchannel based fuel cells.<sup>10,11</sup> Their presence in the cardiovascular system, often described as air embolism, can engender cardiac arrests in some situations.<sup>12</sup> Interestingly, excess drought can also cause air embolism to appear in the transport system of plants, resulting in them drying up and wilting.<sup>13</sup>

When they are small enough, gas bubbles can stably exist on solid surfaces due to the action of surface tension notwithstanding buoyancy. This makes them appear similar to sessile drops. While their removal from surfaces has the potential to speed up boiling,<sup>14</sup> there is increasing interest to insert an intervening gaseous phase between the liquid and solid phases to affect the speed of liquid flow.<sup>15–17</sup> Various

ways to generate bubbles in a flow channel have been reported. These include the use of coflows,<sup>18</sup> ultrasonics,<sup>19</sup> and heating.<sup>20</sup> The methods mentioned, however, may not be suited for locating arrays of gas bubbles precisely on solid surfaces. In the case of drops, the dispensation of liquid using a retracting tip offers a ready means to achieve this.<sup>21</sup>

It is often believed that a gas bubble is complementary to a sessile drop when dispensed on the same surface since the forces acting at the three-phase contact line at equilibrium, according to Young, should be the same. Studies, however, have indicated that the extent of hysteresis between the two can vary significantly.<sup>22,23</sup> Recently, the dispensation of air and liquid on solid surfaces dispensed at fixed volumes of 6  $\mu\text{L}$  was conducted on silicone and silane coated glass surfaces with the dispensing tip retracted at different speeds to test the complementary behavior.<sup>24</sup> With liquid bridges, increasing the retracting speed left behind lower volumes on the substrate. The pinch-off position and the contact line radius were factors that determined these volumes. The bridge first entered into a

Received: January 15, 2014

Revised: May 5, 2014

Published: May 8, 2014



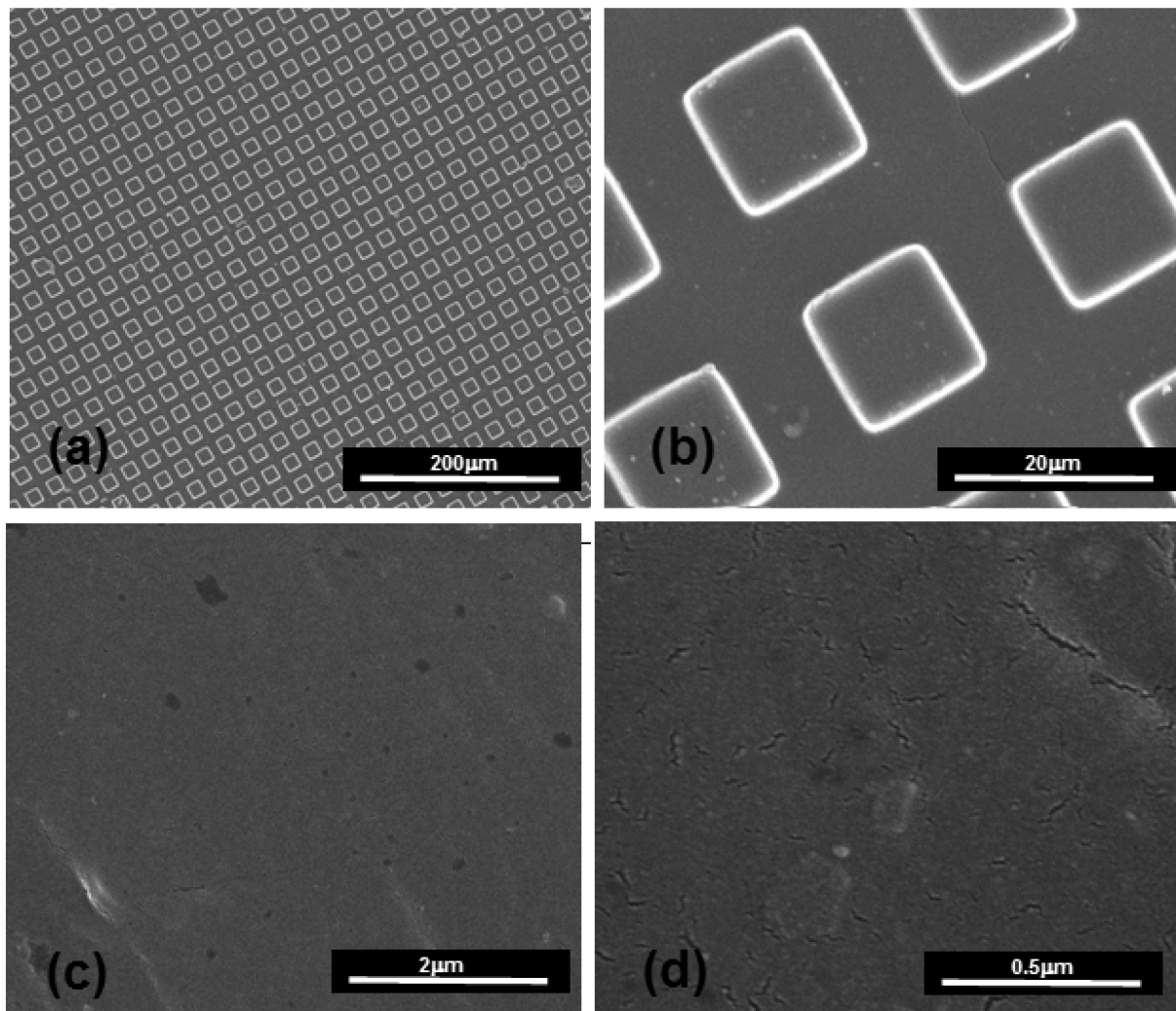


**Figure 1.** Typical SEM images of the structured PDMS surface at (a) low and (b) high magnification which shows organized array of micropillars. Similar typical SEM images of the silicone substrate show no structures at (c) low magnification but at (d) high magnification display the presence of copious nanoscale cracks.

receding state before being able to restore toward equilibrium in a relaxation process closer to rupture. With gas bridges, only a very small volume was left behind on the silane coated glass while the volume deposited on silicone could be tuned from almost none at low retraction speeds to virtually the entire gaseous volume bridge at high retraction speeds. During the progress toward rupture for the gaseous bridge, the contact angle advanced rather than receded, and there was no relaxation stage that brought the contact angle back toward equilibrium before rupture.

Hydrostatic pressure is a well-known factor affecting the function of various phenomena involving liquids.<sup>25,26</sup> For a liquid sessile drop, the variation in hydrostatic pressure can be attained using different volumes. This has been shown to have some effects on the rupture of liquid bridges.<sup>27</sup> Naturally, the ambient pressure can also be altered if experiments are conducted in microgravity. Due to the difficulties in achieving such environments, the use of rotation offers one means of simulation.<sup>28</sup> Nevertheless, some attempts to observe the behavior of bubbles in zero gravity environment created by the free-falling of an aircraft have also been reported.<sup>29</sup> In the context of a gas bubble attached on a surface, the dispensed volume can be kept constant while the depth of liquid changed

to significantly alter the hydrostatic pressure acting on it. This provides an exciting way to investigate the mechanics of bubble formation and dispensation as the tip from which the air was delivered is retracted at constant speeds.

## MATERIALS AND METHODS

**Surface Preparation and Characterization.** Siloxane based polymers, or their more common term of silicones, are widely used in industry due to their typical inherent hydrophobic nature.<sup>30</sup> A popular siloxane based polymer is poly(dimethylsiloxane) (PDMS). Since siloxane based polymers are inherently hydrophobic, the introduction of micro- and nanoscale features can render them superhydrophobic.<sup>31</sup> Two substrates were used, a silicone slide and a surface patterned PDMS piece. The silicone slide was created out of attaching a piece of flat nonpatterned silicone tape (Stylus Tapes International), with adhesive on one side, onto a glass slide. The structured surface PDMS piece was created via a casting process from a silicon master that comprises ordered arrays of square micropillar structures with side lengths of 10  $\mu\text{m}$ , and located 20  $\mu\text{m}$  from each other (center to center).

To create the master, an aligner-exposure system (Karl Suss MA6, Germany) was first used to image the micropillar patterns from a mask onto a silicon wafer. Following this, a deep etching process (STS ICP ASE, U.K.) was introduced to form the structures in 3D. PDMS was

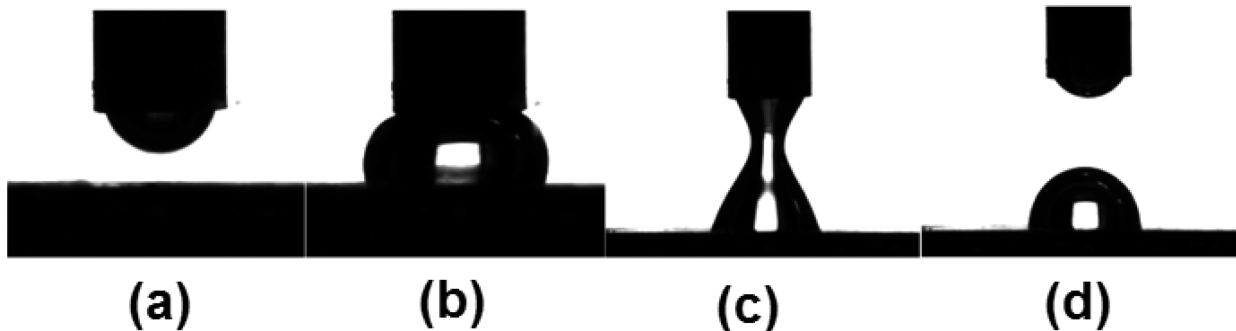


**Figure 2.** Sequence of images of (a) air injected to begin forming a bubble from the tip, (b) the air bubble contacting the substrate and forming to its full intended volume, (c) the tip retracted to form a narrowing neck on the gaseous bridge, and (d) rupture of the bridge to leave a bubble on the substrate.

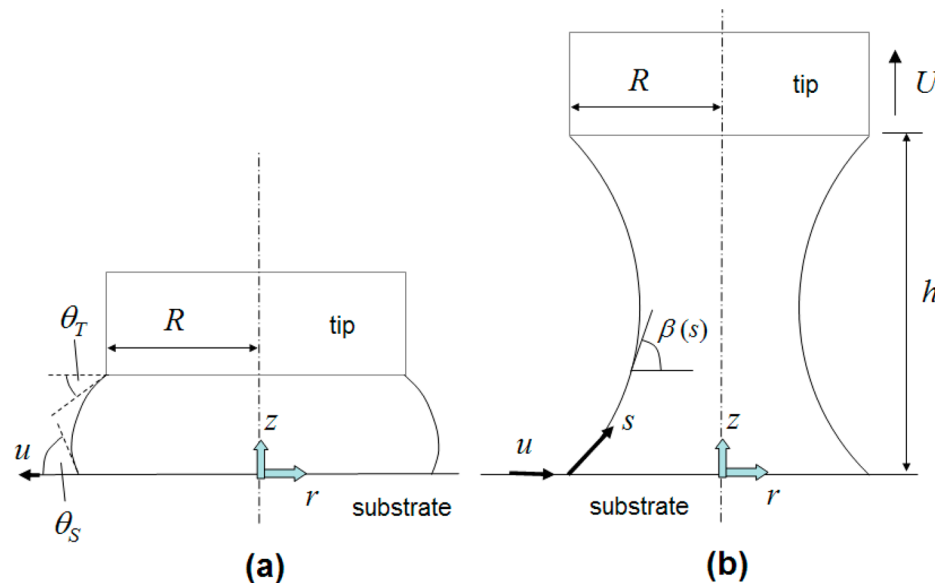


**Figure 3.** Schematic depiction of the bubble deposition process, which can be broken up into two stages, where (a) is the growth of the gaseous phase from the stationary tip, and (b) the rupture of the gaseous bridge when the tip is retracted. The coordinate system and geometry for both cases are shown. The key parameters are the radius of the tip  $R$ , the radius that the bubble makes with the substrate  $r$ , the separation distance between tip and substrate  $h$ , and the contact angles developed at the substrate and tip which are  $\theta_s$  and  $\theta_T$ , respectively.

prepared by mixing with precursor liquid and curing agent (at 10:1 ratio w/w) and then poured onto the micropillar laden master, followed by curing at 70 °C for about 2 h in a vacuum to eliminate air bubbles. After curing, this PDMS film was peeled off the silicon master and oxidized (for 30 s) in O<sub>2</sub> plasma (Plasmatech) to render the surface hydrophilic. It was then placed into a sealed container together with a piece of glass coated with about 20 μL of silane (Sigma-Aldrich, U.S.). The container was evacuated with a vacuum pump and maintained at low pressure for 12 h. This film now contains inverse imprints of the master.

A similar second step of creating the PDMS film containing positive imprints of the micropillars on the master was done by pouring PDMS mixed with precursor liquid and curing agent (at 10:1 ratio w/w) onto the negative PDMS film. After curing for about 2 h at 70 °C, it was then peeled off and oxidized (for 30 s) in O<sub>2</sub> plasma to make the surface hydrophilic. This hydrophilic PDMS stamp was then placed in a sealed container together with a piece of glass coated with about 20 μL of silane. The container was evacuated with a vacuum pump and maintained for 12 h.

The structures on both surfaces were visualized using scanning electron microscopy (SEM) imaging. As the substrates were dielectric, they were coated with a thin layer of gold to avoid charging. Following this, they were placed inside a scanning electron microscope (FEI

Quanta 3D FEG) in which the electron beam voltage applied was 10 kV, and images were recorded at magnifications of up to 100 000×.

**Bubble Dispensation Studies.** The bubble dispensation studies were conducted on a drop shape analysis system (Kruss DSA100). The syringe had a 500 μL capacity and a flat tip of 2 mm outer diameter and 1.6 mm inner diameter that was made of stainless steel. Stainless steel is known to have contact angle between 70° and 75° with water. During the experiments, the temperature was recorded at 22 °C.

The dispensed volume bubble was kept at 6 μL throughout the experiments, with the needle kept at the height of 1 mm above surface. The dispensation of air from the needle was made using a flow rate of 5 μL/s. After the bubble was allowed to settle for 10 s, the needle tip was retracted at a speed of 1 mm/s. After bubble rupture, the volume of bubble retained on the surface was calculated by assuming that its shape was semispherical and axis symmetric. In the experiments, a plastic transparent container with dimension of 87 × 87 × 75 (width × length × height in mm) was used to serve as water reservoir. The container was filled with water to heights ranging from 10 to 50 mm in 5 mm increments to vary the hydrostatic pressure.

The entire deposition and rupture processes of microbubble/droplet were recorded using the DSA100s built-in camera. The lens was laser guided to align at 90° with the needle tip to prevent any projection from occurring in measurement. The variations in contact

angle, contact line, rupture height, and volume of the microbubble and droplet were investigated.

An open source analysis software Tracker ([www.cabrillo.edu/~dbrown/tracker/](http://www.cabrillo.edu/~dbrown/tracker/)) was used to process the video sequences. Contact angle and contact line measurements were done by tracking three points on each side of the microbubble/droplet at the contact region during the deposition and rupture processes.

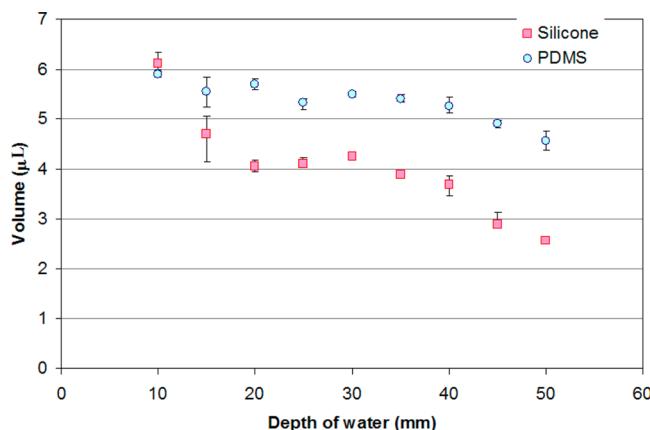
## RESULTS AND DISCUSSION

Figure 1 presents SEM images of the structured PDMS surface at (a) low and (b) high magnification. They confirm presence of an organized array of micropillars obtained from the fabrication process. We interrogated other regions of the sample and found no departure in the patterns. The SEM image of the silicone substrate at (c) low magnification revealed no microscaled structures. At higher magnifications (d), however, a copious presence of nanoscale cracks, some as short as 50 nm in length, could be seen. Microscale cracks have been observed previously in treated soft polymers and attributed to the action of residual strain from applied physical forces.<sup>32</sup> It is conceivable that the nanoscale cracks here may have developed in a similar fashion when the silicone tape was manufactured.

Figure 2 provides a sequence of images that make up the bubble deposition process. The tip, when immersed into the liquid initially, will experience a bubble forming (a) as air is injected into it. The growing air bubble contacts the substrate to form a bridge and reaches its intended volume (b). When the tip is retracted, a neck appears on the gaseous bridge (c), which narrows with greater tip retraction, and eventually ruptures to leave behind a bubble on the substrate as well as on the tip (d).

Clearly, the process can be broken up into two major stages (as depicted in Figure 3) comprising (a) the growth of the gaseous phase from the stationary tip with air injection and (b) the steps leading to the rupture of the gaseous bridge when the tip was retracted. In both stages, the contact line associated with the tip was stationary whereas that on the substrate was movable. The contributions of the Weber, Bond, and capillary dimensionless numbers should be pertinent, since they each represent the relative importance of inertial force/surface tension, gravity/surface tension, and viscous force/surface tension, respectively. The small Bond number of  $Bo = g\rho R^2/\gamma \sim O(10^{-4})$  operational in the experiments, where  $g$  is gravitational acceleration,  $\rho$  is liquid density,  $R$  is tip radius, and  $\gamma$  is surface tension of water, indicated that the action of gravity was insignificant. The flow speed inside the bridge is on the order of the speed of the tip  $U$ . Consequently, with  $\mu$  as viscosity, and the capillary wave speed as  $u_{cp} = \sqrt{\gamma/\rho R}$ , the orders of the Weber and capillary numbers were  $We = \rho u_{cp}^2 R/\gamma \sim O(1)$  and  $Ca = \mu u_{cp}/\gamma \sim O(10^{-2})$ . These values indicate that while the inertial forces in action were comparable in magnitude to the surface tension, the viscous forces were lower. To be assured that dissolution was not an operating mechanism in the experiments, a sample bubble of measured volume 4.3  $\mu L$  was deposited on a substrate and left for 240 s at 50 mm H<sub>2</sub>O hydrostatic pressure. It was found that the volume was unchanged when measured after this period.

Figure 4 provides plots of bubble volumes deposited on the structured PDMS and silicone substrates, respectively. It can be seen that greater volumes could be left behind on the structured PDMS substrate arising from the process. Interestingly for hydrostatic pressures up to 20 mm H<sub>2</sub>O, there were



**Figure 4.** Plots of bubble volumes deposited on the structured PDMS and silicone substrates. Greater volumes could be left behind on the structured PDMS substrate. Up to 20 mm H<sub>2</sub>O (196 Pa), hydrostatic pressure did not seem to affect this volume. For depths above 30 mm H<sub>2</sub>O (294 Pa), the volume of bubble that could be left behind progressively decreased. The error bars indicate the maximum and minimum values taken from five readings.

no significant effects on the deposited bubble volume on either substrate. With the structured PDMS substrate, virtually all the air volume introduced was left on it after rupture. At pressures above 20 mm H<sub>2</sub>O, however, the volume of bubble deposited was found to decrease progressively. This clearly shows the influence of hydrostatic pressure, since the retraction speed of the tip was kept constant throughout.

We extracted information on the contact widths ( $2r$ ) and heights ( $ht$ ) of the bubble on the respective substrate surfaces based on the results in Figure 4 and plotted them in Figure 5.

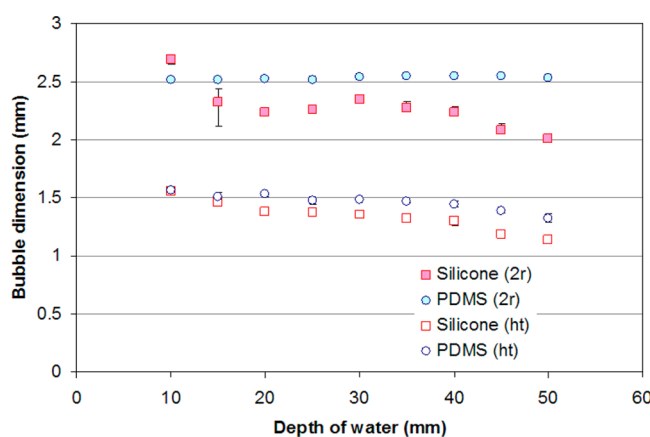


**Figure 5.** Plots of the deposited bubble widths ( $2r$ ) and heights ( $ht$ ) on the structured PDMS and silicone surfaces. Reducing trends with hydrostatic pressure (in which 10 mm H<sub>2</sub>O = 98 Pa) are evident. Between the two substrates, the differences in height were marginal while they were significant in width. The error bars indicate the maximum and minimum values taken from five readings.

Both contact width and height had reducing trends with pressure increase, indicating the influence of both the factors in affecting the deposited volume when hydrostatic pressure was increased. In comparison, the differences in height were marginal compared to that of the contact width at any particular hydrostatic pressure. Nevertheless, since both contact width and height altered with pressure change this observation

does not offer any conclusive generalizations. What is evident is the ability of hydrostatic pressure to influence the extent to which the contact line moved during the tip retraction process. This movement should then play a role in determining the volume that is left behind on the surface following rupture. Clearly, better insights can be attained by inspecting the time based dimensional evolutions of the bubble more closely.

Figure 6 presents plots of the height of gaseous bridge from the substrate surface ( $h$ ) for structured PDMS and silicone

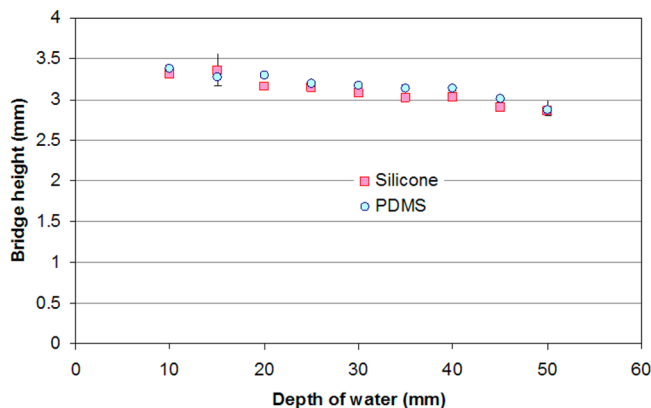


**Figure 6.** Plots of the gaseous bridge height ( $h$ ) attained before rupture on structured PDMS and silicone during tip retraction at various hydrostatic pressures (in which  $10 \text{ mm H}_2\text{O} = 98 \text{ Pa}$ ). The trends are linearly decreasing with increasing hydrostatic pressure. The error bars indicate the maximum and minimum values taken from five readings.

attained just before rupture. It can be seen that the trends were linearly decreasing with hydrostatic pressure, at a rate of approximately  $0.012 \text{ mm/Pa}$ . These results then help to explain the reduction trend in the volume dispensed on the substrate surface with hydrostatic pressure (see Figure 4). In the case of cylindrical shaped liquid bridges, the classical Rayleigh limit dictates that stability is lost when its length is larger than its perimeter. This may be modified by the influence of different parameters.<sup>33–35</sup> We have previously indicated that when a gaseous bridge ruptures, it does not follow the situation in which material is thinned out at the necking point as in the case of the liquid bridge.<sup>24</sup> Rather, one can think of the process more in terms of the liquid phase moving in to try to displace the gaseous phase that separates them. The manner in which this happens parallels somewhat the situations where sessile drops collide with each other<sup>36</sup> or two liquid bodies coalesce to create a bridge leading to mixing.<sup>37</sup> From an energy perspective, when a gaseous bridge is created, the surface energy  $\Delta\Omega_s$  is related to the liquid–vapor surface tension  $\gamma$  and the surface areas of the liquid–vapor interface  $A_{LV}$  on the substrate  $A_s$  and on the tip  $A_T$  via

$$\Delta\Omega_s = \gamma[A_{LV} - A_s \cos(\theta_s) - A_T \cos(\theta_T)] \quad (1)$$

The total energy  $\Delta\Omega_{\text{tot}} = \Delta\Omega_s + \Delta\Omega_v$  is then a simple sum of the surface energy and the volume energy  $\Delta\Omega_v$ . During the phase when the tip is retracted,  $\Delta\Omega_v$  is constant while  $\Delta\Omega_s$  changes. Since the volume energy remains relatively constant, the increase in  $A_{LV}$  imbues additional energy. Since the system generally favors energy minimization, an increase in the overall energy will drive the bridge toward instability from which rupture will be an avenue for the system to restore to a lower energy state. It is important to note that in the lead up to

rupture, the neck region can be taken to comprise two roughly conical sections. Within the height of the bridge, the presence of a hydrostatic pressure gradient will cause an up–down asymmetry in the two conical sections. Simulations have confirmed this in the case of bubbles pinching off due to injection of air from the base.<sup>38</sup> The higher pressure closer to the base should cause the gas volume to preferentially gravitate toward the tip (see Figure 7). When the overall hydrostatic

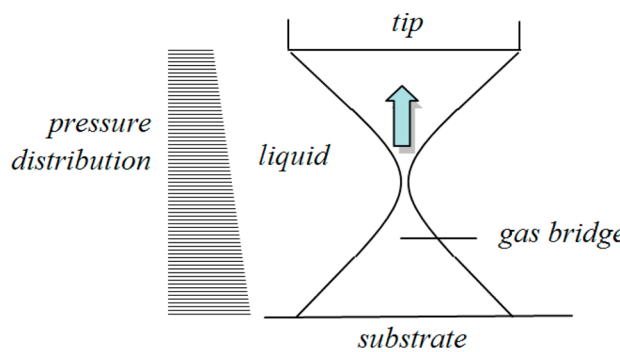


**Figure 7.** During tip retraction, the neck region can be approximated by two cones. With a pressure gradient, the higher pressure closer to the base will tend to cause more volume on the bridge to move toward the tip (as indicated by the arrow). However, it takes a higher absolute pressure to move the rupture point closer to the substrate such that a greater volume resides at the tip.

pressure is high, it is likely that during the onset of instability the rupture point is able to shift downward toward the substrate. Consequently, this should leave a smaller volume there and a larger volume at the tip. It is important to note that this process is aided by inertial forces (due to buoyancy) which have been established here to be of the same order of magnitude as the surface tension forces. One would then expect that this asymmetry to be an additional source of instability on the bridge, a fact that has also been established in the case of bubble pinch-off from injection.<sup>39</sup> This is corroborated by the results here, which indicate that a higher hydrostatic pressure tended to cause a faster onset of instability and rupture of the gaseous bridge. Interestingly, the preferential movement of the bridge volume toward the tip has potential positive implications in the creation of flows that do not need the use of pumps to create pressure differentials across the fluid medium.<sup>40</sup>

The height of the gaseous bridge attained before rupture, however, does not provide a direct explanation of the volume dispensation behavior between the two substrate surfaces. At hydrostatic pressure of  $50 \text{ mm H}_2\text{O}$  for instance, the heights before rupture on structured PDMS and silicone were 1.34 and 1.8 mm, respectively. Nevertheless, the volumes deposited on them were 4.3 and  $2.3 \mu\text{L}$  (see Figure 4) respectively. It will be necessary to consider at least another dimension of the gaseous bridge that contributes to changes in the volume dispensed arising from rupture to account for this.

Figure 8 furnishes plots of the contact angle ( $\theta_s$ ) that the gaseous bridge makes with the substrate surface for (a) structured PDMS and (b) silicone during tip retraction at various hydrostatic pressures. For structured PDMS at 35 and 50 mm  $\text{H}_2\text{O}$  hydrostatic pressure, the contact angle remained somewhat constant throughout at around  $130^\circ$ , despite some fluctuations, as the tip was retracted to the point of gaseous bridge rupture. In the case with  $10 \text{ mm H}_2\text{O}$  hydrostatic pressure, the contact angle increased to that value from an

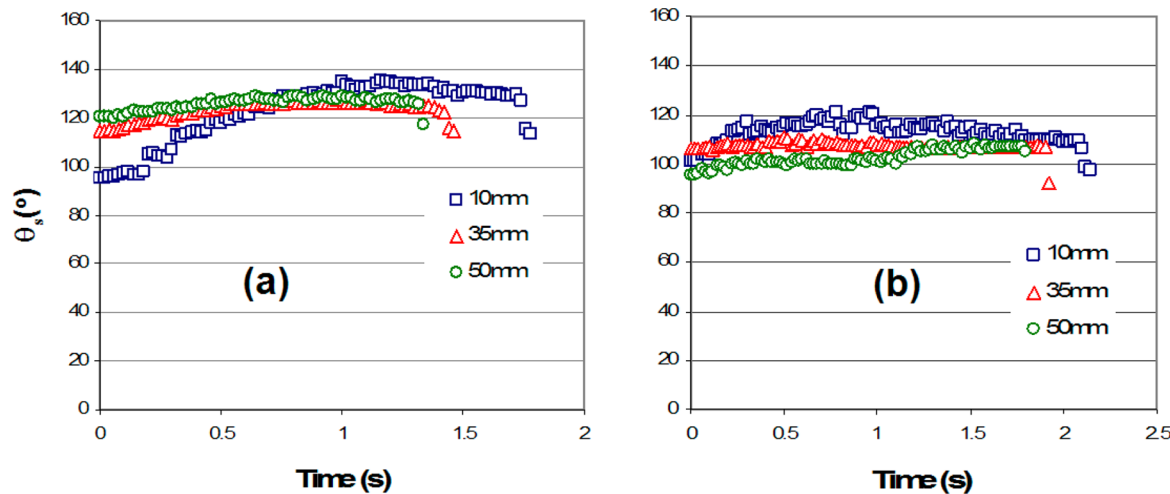


**Figure 8.** Plots of the contact angle ( $\theta_s$ ) that the gaseous bridge makes with the substrate surface for (a) structured PDMS and (b) silicone during tip retraction at various hydrostatic pressures in terms of water level depths. While there are fluctuations, the overall trend is one in which the limiting receding value is maintained in the lead up to rupture. In conversion, 10, 35, and 50 mm H<sub>2</sub>O are 98, 343, and 490 Pa, respectively.

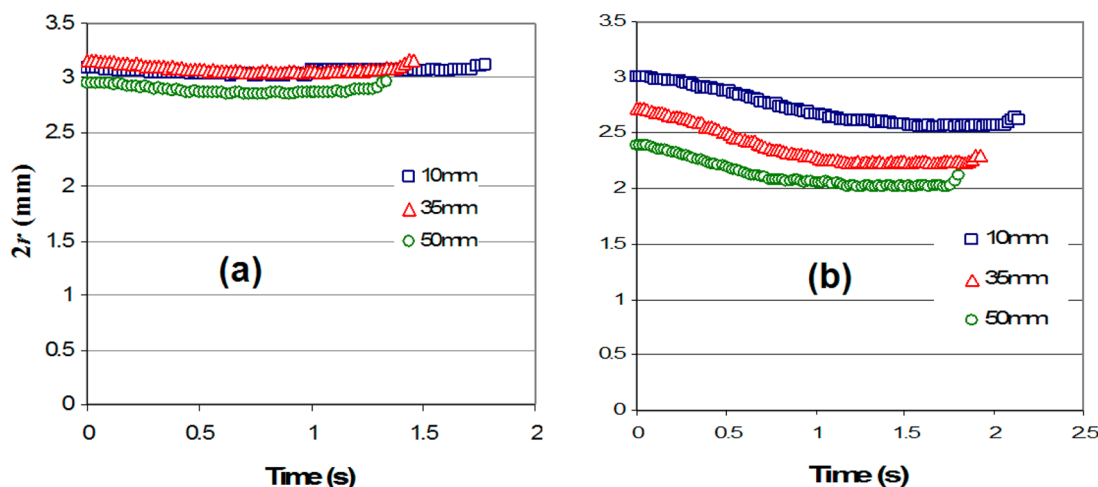


**Figure 9.** Plots of gaseous bridge width ( $2r$ ) contact on the substrate surface for (a) structured PDMS and (b) silicone during tip retraction at various hydrostatic pressures in terms of water level depths. On structured PDMS, the width trends are invariant with time and are not affected by hydrostatic pressure. On silicone, the gaseous bridge width initially reduced with time before becoming invariant in the lead up toward rupture and assumes smaller magnitudes with higher hydrostatic pressure. In conversion, 10, 35, and 50 mm H<sub>2</sub>O are 98, 343, and 490 Pa, respectively.

initial value of 100°. We attribute this to a particular instance during the growth stage where there was some additional pinning on the surface due to unintended nonheterogeneities present. Yet the contact angle was able to adjust to a relatively constant angle later despite this. In the case of silicone, the trends were constant as well, albeit having a lower value of around 105°. These constant value trends, as well as their assuming the same value at the point of rupture according to substrate type, impinge that this factor did not contribute much toward directly dictating the bubble volume dispensed on the surface.

Figure 9 provides plots of the gaseous bridge contact width ( $2r$ ) on the substrate surface for (a) structured PDMS and (b) silicone during tip retraction at various hydrostatic pressures. On structured PDMS, one finds the width trends to be rather invariant with time as well as having magnitudes relatively unaffected by hydrostatic pressure. These results show that the contact line was strongly pinned on the structured PDMS surface during the tip retraction stage. If we correlate this with Figure 8a, where the contact angle remained relatively invariant

as well, it can be deduced that significant curvature changes ought to have occurred near the neck region. On the silicone substrate alternatively, the gaseous bridge width initially reduced with time before becoming invariant in the lead up to rupture. This indicated that during the early stages of tip retraction, the contact line was able to undergo movement before being fixed. Normally, such a transition is associated with strong contact angle changes. As the contact angle remained relatively constant (see Figure 8b), it also implies significant curvature changes near the neck region in the lead up to rupture. It is apparent then that in the case of silicone, the reduction in width and height from the surface with increase in hydrostatic pressure contributed to the volume changing trends observed in Figure 4b. In the case of structured PDMS, only the height from the surface contributed to the volume change trends observed in Figure 4a. This then explains the ability of the structured PDMS to yield larger volume depositions as compared to silicone. At this juncture, it is pertinent to mention that the contact angle for the structured PDMS (130°) is larger than that for silicone (105°). Higher contact angles often imply

greater ease of motion of the contact line which in turn imparts greater mobility. However, it has been pointed out that contact angles are in fact a manifestation of three forces acting in equilibrium according to Young's equation and do not take into account actual adhesion.<sup>41</sup> In other words, it is possible for greater adhesion to occur notwithstanding larger contact angles being manifested by either the drop or the bubble.

On closer examination of Figure 9b, it can be seen that the widths were smaller at the start of the tip retraction process when the hydrostatic pressure was greater. For instance, the starting widths at hydrostatic pressures 10 and 50 mm H<sub>2</sub>O were 3 and 2.4 mm, respectively. Despite the presence of varied hydrostatic pressures during tip retraction, the reduction in width was approximately 0.5 mm in all cases. These trends were not observed at all on the structured PDMS substrate (see Figure 9a). In the case of the silicone substrate, hence, it is clear that increased hydrostatic pressure likely restricted the width growth of the gaseous bridge during the stage when air was injected in through the tip, and it is this factor that essentially determined the differentiation in width of the gaseous bridge on the substrate just before rupture at different hydrostatic pressures. This situation can also be understood from considering the energies involved. Since the bubble is strongly pinned at the tip, it is the contact line evolution on the substrate that is most pertinent. The work done  $\delta w$  associated with growth can be related to the respective liquid–vapor, solid–liquid, and solid–vapor surface tensions  $\gamma$ ,  $\gamma_{SL}$ ,  $\gamma_{SV}$ ; liquid–vapor, solid–liquid, and solid–vapor area changes  $dA_{LV}$ ,  $dA_{SL}$ ,  $dA_{SV}$ ; Laplace pressure change  $\Delta P$ , and volume change  $dV$  via

$$\delta w = \gamma dA_{LV} + \gamma_{SL} dA_{SL} + \gamma_{SV} dA_{SV} + \Delta P dV \quad (2)$$

Let us consider the start situation when the bubble first contacts the substrate surface. At this state, we can assume that all the areas to be the same, whether on the patterned PDMS or silicone substrate. When growth just begins, the first and fourth terms on the right of eq 2 should be the same. Let us make a simple assumption of incompressibility of both fluids. This dictates that  $dA_{SV} = -dA_{SL}$  and simplifies the second and third terms on the right to  $dA_{SV}(\gamma_{SL} - \gamma_{SV})$ . For the same value of  $\delta w$ , hence, higher values of  $\gamma_{SL} - \gamma_{SV}$  will cause smaller values of  $dA_{SV}$  and vice versa. With smaller values of  $dA_{SV}$ , the width in contact with the substrate at the end of growth should be correspondingly smaller. Since this width reduces with hydrostatic pressure on the silicone substrate, it will be reasonable to infer that the key lies in changes to  $\gamma_{SL} - \gamma_{SV}$ . In experiments using nanoparticles in the liquid medium, it has been previously found and argued that higher liquid pressures generated at the three-phase contact line increase wettability, or essentially the difference between  $\gamma_{SL}$  and  $\gamma_{SV}$ <sup>42</sup> (see Figure 10a). If applied in our case, this translates to smaller values of  $dA_{SV}$  when the hydrostatic pressure is greater, therefore accounting for the reduction in contact widths that was found. So why does not this apply to the case of patterned PDMS? We contend that the regular structures offer the possibility of a higher proportion of Cassie wetting states and thus cause a weaker tendency of the liquid phase to travel into the gaseous phase at the contact line (see Figure 10b). In digressing a little, this mechanism also fosters bubbles with the ability to exist at larger volumes than expected on superhydrophobic surfaces as reported previously.<sup>23</sup> When this happens,  $\gamma_{SL} - \gamma_{SV}$  remains approximately invariant notwithstanding the hydrostatic pressure change.

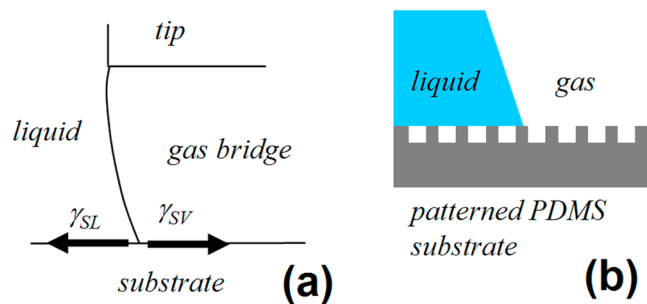


**Figure 10.** From the initial stage of bubble growth on the substrate (a) the extent to which the solid–vapor area is able to change is dependent on the solid–vapor  $\gamma_{SV}$  surface tension and the solid–liquid  $\gamma_{SL}$  surface tension. Hydrostatic pressure should be able to affect this difference in general. This will ascertain the width of the gas bridge coming in contact with the substrate at the end of the growth. In the case of patterned PDMS (b), the features on the substrate surface permit a higher proportion of the Cassie wetting state, which then make the  $\gamma_{SL} - \gamma_{SV}$  to be relatively immune to the effect of hydrostatic pressure.

In following the growth stage of the gaseous bridge (as air was injected through the tip) on the silicone substrate at hydrostatic pressure of 50 mm H<sub>2</sub>O, plots of the contact angle at the substrate surface ( $\theta_s$ ) (see Figure 11a) show increases with time before reaching a constant value (at 0.5 s from the start of record coinciding to the situation where air stopped being injected in through the tip). The plot in Figure 11b of the gaseous bridge width ( $2r$ ) development on the substrate shows an increase with time before reaching a constant value. The strong linear trend indicates that the contact line was moving at an almost constant speed. The high degree of fluctuation in  $\theta_s$  values during this process indicates a series of pinning and depinning processes, which have been observed previously when a liquid bridge was moved through a strongly hydrophobic surface in which the overall contact angle remained somewhat fixed.<sup>43,44</sup> In the situation here, the stochastic pinning and depinning proceeded even as the gaseous bridge was deforming to change  $\theta_s$  in order to accommodate the additional input of air. Since there was no neck appearing on the bridge during this stage, it is likely that there would be contact angle changes at the tip ( $\theta_T$ ) in order to accommodate the contact angle and width changes at the substrate. This is confirmed in Figure 11a, where we see the tip contact angle exhibiting reduction with time before reaching a constant value. In this case, the fluctuations were much smaller than in the case of  $\theta_s$ , which indicates much lower instances of pinning and depinning on the tip. This can be attributed to the known ability of the edges to accommodate higher levels of hysteresis.<sup>45,46</sup> It is also important to note that all three parameters ( $\theta_s$ ,  $\theta_T$ , and  $2r$ ) altered from a varying state to a constant state simultaneously at around 0.5 s from the start of recording, indicating their tandem operation to determine the gaseous bridge morphology.

We discuss some applied implications from the findings here. The aquatic beetle *Potamodytes tuberosus* has a gaseous bubble that conspicuously hangs from its body underwater which it uses for respiration. This beetle is almost never found in locations of slow moving or stagnant water. It has been claimed that the liquid flow permits the bubble to grow or maintain its size dynamically through the action of Bernoulli's principle.<sup>47</sup> We ruminated previously that the insect could harness the rock surface to temporarily create a stable gaseous bridge that grew

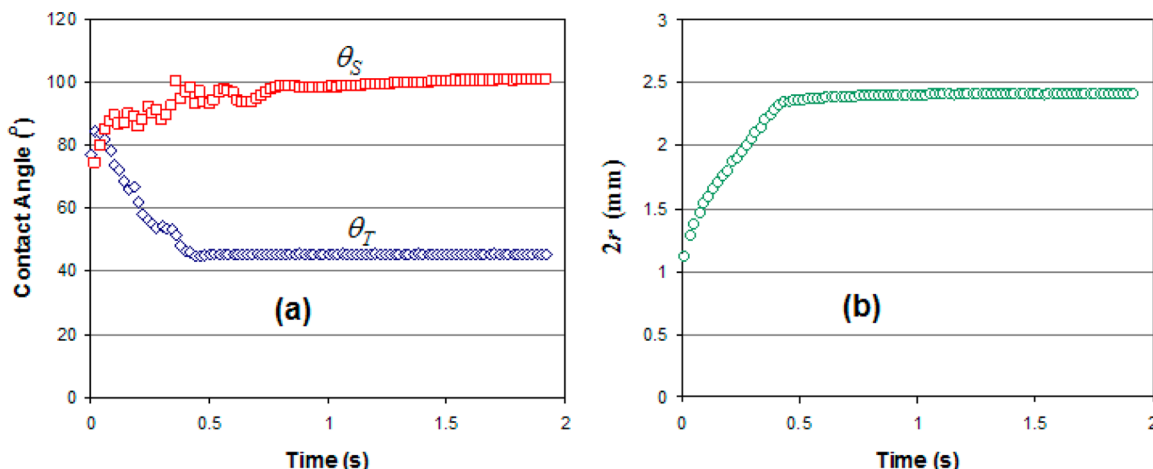


**Figure 11.** During the growth stage of the gaseous bridge on the silicone substrate at hydrostatic pressure of 50 mm H<sub>2</sub>O (490 Pa), plots of (a) the contact angle at the substrate surface ( $\theta_s$ ) show increases with time before being constant, while the contact angle at the tip ( $\theta_T$ ) display reduction with time before being constant. The plot (b) of the gaseous bridge width ( $2r$ ) on the substrate shows an increase with time before being constant. Air was injected through the tip until 0.5 s from the start of record.

stably and subsequently could be detached from, notwithstanding the flow of the surrounding fluid.<sup>24</sup> Based on the findings here, it is plausible that diving to greater depths (where the hydrostatic pressure is greater) may also be used as a strategy to retain higher gaseous volume on its body in the process.

This mechanism comes to play as well in another scenario of creating arrays of bubbles on surfaces using the tip retraction process. It may not be possible to create large enough volumes when the hydrostatic pressure is too high. The findings here indicate that a simple solution will be to first draw out an amount of liquid from the container, create the bubbles on the substrate under lower hydrostatic pressure, and then restore the liquid back into the container. It should also be noted that recent investigations have found bubbles on surfaces to be affected by electrowetting.<sup>48</sup> This potentially affords the means to change the shape of bubbles on surfaces, making it versatile in the creation of lab-on-a-chip devices. In the first instance, having a bubble with the right size will be desirable.

## CONCLUSIONS

We investigated the effect of hydrostatic pressure on 6  $\mu\text{L}$  air bubbles formed on structured PDMS and silicone using a 2 mm diameter stainless steel tip that was retreated at 1 mm/s. SEM imaging showed the structured PDMS surface to possess an organized array of micropillars while the silicone surface had a copious presence of nanoscale cracks which were likely developed out of residual strain. From dimensional analysis, the tip retraction process involved the inertial forces in action to be comparable in magnitude to the surface tension forces, while the viscous forces were lower. Larger bubbles could be left behind on the structured PDMS surface generally. Hydrostatic pressures up to 20 mm H<sub>2</sub>O (196 Pa) had no significant effect on the deposited bubble volume on both substrates. Above this pressure, however, the volume of bubble deposited was found to decrease progressively. The differences in height of the deposited bubbles at any particular hydrostatic pressure were marginal, but they were significant in width. Increases in the hydrostatic pressure reduced the attainable height attained before rupture, and thus accounted for the reducing dispensed volume trend. On structured PDMS, the gaseous bridge width was invariant with tip retraction; however,

on silicone, it was initially reducing before becoming invariant in the lead up to rupture. In the case of silicone, both reductions in width and height with increase in hydrostatic pressure likely contributed to the volume changing trends, thereby accounting for why the deposited volumes were smaller on silicone than on the structured PDMS surface. With the silicone substrate, increased hydrostatic pressure was also found to restrict the growth in contact width of the bridge during the stage when air was injected in through the tip. In following the growth stage of the gaseous bridge (as air was injected through the tip) on the silicone substrate at constant hydrostatic pressure, the contact width increase trend development was linear, indicating that the contact line was moving at an almost constant speed. The high degree of fluctuation in  $\theta_s$  values during this process indicated a pinning and depinning process even as the gaseous bridge was deforming to change  $\theta_s$  in order to accommodate the input of air. The affect of hydrostatic pressure on the deposited volume of bubbles on surfaces found here offers useful ways to interpret mechanisms in nature and to be harnessed for desired applications.

## AUTHOR INFORMATION

### Corresponding Author

\*E-mail: engngtw@gmail.com. Telephone: 61-3-99054647. Fax: 61-3-99051825.

### Notes

The authors declare no competing financial interest.

## ACKNOWLEDGMENTS

T.W.N. acknowledges funding from the Australian Research Council Discovery Project DP120100583. Y.Y. appreciates funding support from the Beijing Higher Education Young Elite Teacher Project. Access to usage of facilities at the Melbourne Center for Nanofabrication and the Kruss DSA100 system at the Institute of Frontier Materials, Deakin University is appreciated. Discussions with A.M. Richards and O.W. Liew at the Cardiovascular Research Institute, Singapore, are also noted.

## ■ REFERENCES

- (1) Betz, A. R.; Attinger, D. Can segmented flow enhance heat transfer in microchannel heat sinks? *Int. J. Heat Mass Transfer* **2010**, *53*, 3683–3691.
- (2) Kao, J.; Wang, X.; Warren, J.; Xu, J.; Attinger, D. A bubble-powered micro-rotor: Conception, manufacturing, assembly, and characterization. *J. Micromech. Microeng.* **2007**, *17*, 2454–2460.
- (3) Choi, H.-J.; Montemagno, C. D. Biosynthesis within a bubble architecture. *Nanotechnology* **2006**, *17*, 2198–2202.
- (4) El-Ali, J.; Gaudet, S.; Gunther, A.; Sorger, P. K.; Jensen, K. F. Cell stimulus and lysis in a microfluidic device with segmented gas–liquid flow. *Anal. Chem.* **2005**, *77*, 3629–3636.
- (5) Cox, D. J.; Thomas, J. L. Temperature-dependent biphasic shrinkage of lipid-coated bubbles in ultrasound. *Langmuir* **2013**, *29*, 4485–4491.
- (6) Qin, S.; Caskey, C. F.; Ferrar, K. W. Ultrasound contrast microbubbles in imaging and therapy: Physical principles and engineering. *Phys. Med. Biol.* **2009**, *54*, R27.
- (7) Ling, W. Y. L.; Ng, T. W.; Neild, A. Effect of an encapsulated bubble in inhibiting droplet sliding. *Langmuir* **2010**, *26*, 17695.
- (8) Ling, W. Y. L.; Ng, T. W.; Neild, A.; Zheng, Q. Sliding variability of droplets on a hydrophobic incline due to surface entrained air bubbles. *J. Colloid Interface Sci.* **2010**, *354*, 832–842.
- (9) Jensen, M. J.; Goranovic, G.; Bruus, H. The clogging pressure of bubbles in hydrophilic microchannel contractions. *J. Micromech. Microeng.* **2004**, *14*, 876–883.
- (10) Kamitani, A.; Morishita, S.; Kotaki, H.; Arscott, S. Miniaturized microDMFC using silicon microsystems techniques: Performances at low fuel flow rates. *J. Micromech. Microeng.* **2008**, *18*, 125019–28.
- (11) Kamitani, A.; Morishita, S.; Kotaki, H.; Arscott, S. Improved fuel use efficiency in microchannel direct methanol fuel cells using a hydrophilic macroporous layer. *J. Power Sources* **2009**, *187*, 148–155.
- (12) Deceuninck, O.; De Roy, L.; Moruzi, S.; Blommaert, D. Massive air embolism after central venous catheter removal. *Circulation* **2007**, *116*, e516–e518.
- (13) Choat, B.; Jansen, S.; Brodrribb, T. J.; Cochard, H.; Delzon, S.; Bhaskar, R.; Bucci, S. J.; Field, T. S.; Gleason, S. M.; Hacke, U. G.; Jacobsen, A. L.; Lens, F.; Maherli, H.; Martínez-Vilalta, J.; Mayr, S.; Mencuccini, M.; Mitchell, P. J.; Nardini, A.; Pittermann, J.; Pratt, R. B.; Sperry, J. S.; Westoby, M.; Wright, I. J.; Zanne, A. E. Global convergence in the vulnerability of forests to drought. *Nature* **2012**, *491*, 752–755.
- (14) Vakarelski, I. U.; Patankar, N. A.; Marston, J. O.; Chan, D. Y. C.; Thoroddsen, S. T. Stabilization of Leidenfrost vapour layer by textured superhydrophobic surfaces. *Nature* **2012**, *489*, 274–277.
- (15) Carlborg, C. F.; Wijngaart, W. v. d. Sustained superhydrophobic friction reduction at high liquid pressures and large flows. *Langmuir* **2011**, *27*, 487–493.
- (16) Steinberger, A.; Cottin-Bizonne, C.; Kleimann, P.; Charlaix, E. High friction on a bubble mattress. *Nat. Mater.* **2007**, *6*, 665–668.
- (17) De Gennes, P. G. On fluid/wall slippage. *Langmuir* **2002**, *18*, 3413–3414.
- (18) Wang, K.; Xie, L.; Lu, Y.; Luo, G. Generating microbubbles in a co-flowing microfluidic device. *Chem. Eng. Sci.* **2013**, *100*, 486–495.
- (19) Makuta, T.; Takemura, F.; Hihara, E.; Matsumoto, Y.; Shoji, M. Generation of micro gas bubbles of uniform diameter in an ultrasonic field. *J. Fluid Mech.* **2006**, *548*, 113–131.
- (20) Prakash, M.; Gershenfeld, N. Microfluidic bubble logic. *Science* **2007**, *315*, 832–835.
- (21) Qian, B.; Breuer, K. S. The motion, stability, and breakup of a stretching liquid bridge with a receding contact line. *J. Fluid Mech.* **2011**, *666*, 554–572.
- (22) Hong, S. J.; Chang, F. M.; Chou, T. H.; Chan, S. H.; Sheng, Y. J.; Tsao, H. K. Anomalous contact angle hysteresis of a captive bubble: Advancing contact line pinning. *Langmuir* **2011**, *27*, 6890–6896.
- (23) Ling, W. Y. L.; Lu, G.; Ng, T. W. Increased stability and size of a bubble on a superhydrophobic surface. *Langmuir* **2011**, *27*, 3233–3237.
- (24) Huynh, H. S.; Guan, J. P.; Vuong, T.; Ng, T. W. Comparisons of micro liquid and gaseous drops deposited on surfaces via a retreating tip. *Langmuir* **2013**, *29*, 11615–11622.
- (25) Extrand, C. W. Repellency of the lotus leaf: Resistance to water intrusion under hydrostatic pressure. *Langmuir* **2011**, *27*, 6920–6925.
- (26) Rahmani, A.; Knight, C.; Morrow, M. R. Response to hydrostatic pressure of bicellar dispersions containing an anionic lipid: Pressure-induced interdigitation. *Langmuir* **2013**, *29*, 13481–13490.
- (27) Wang, X.-W.; Yu, Y. Study of gravitation effect on rupture distance of liquid bridge between two flat substrates. *J. Exp. Mech.* **2012**, *27*, 70–76.
- (28) Bauer, H. F. Damped response of an axially excited rotating liquid bridge in zero-gravity. *Acta Mech.* **1989**, *79*, 295–301.
- (29) Leslie, F. Measurements of rotating bubble shapes in low-gravity environment. *J. Fluid Mech.* **1985**, *161*, 269–279.
- (30) Lebrun, J. J.; Porte, H. Polysiloxanes. In *Comprehensive Polymer Science*; Allen, G., Bevington, J. C., Eds.; Pergamon Press: Oxford, U.K., 1989; pp 593–606.
- (31) Tropmann, A.; Tanguy, L.; Koltay, P.; Zengerle, R.; Rieger, L. Completely superhydrophobic PDMS surfaces for microfluidics. *Langmuir* **2012**, *28*, 8292–8295.
- (32) Mills, K. L.; Zhu, X.; Takayama, S.; Thouless, M. D. The mechanical properties of a surface-modified layer on poly-(dimethylsiloxane). *J. Mater. Res.* **2008**, *23*, 37–48.
- (33) Wang, Y.; Michelsen, S.; Lee, H. J. Symmetric and asymmetric capillary bridges between a rough surface and a parallel surface. *Langmuir* **2013**, *29*, 11028–11037.
- (34) Chen, H.; Amirfazli, A.; Tang, T. Modeling liquid bridge between surfaces with contact angle hysteresis. *Langmuir* **2013**, *29*, 3310–3319.
- (35) Lye, J. K. K.; Ng, T. W.; Ling, W. Y. L. Discrete microfluidics transfer across capillaries using liquid bridge stability. *J. Appl. Phys.* **2011**, *110*, 104509.
- (36) Borcia, R.; Bestehorn, M. Partial coalescence of sessile drops with different miscible liquids. *Langmuir* **2013**, *29*, 4426–4429.
- (37) Cheong, B. H.-P.; Lye, J. K. K.; Backhous, S.; Liew, O. W.; Ng, T. W. Microplates based on liquid bridges between glass rods. *J. Colloid Interface Sci.* **2013**, *397*, 177–184.
- (38) Herbst, D. C.; Zhang, W. W. Underwater bubble pinch-off: Transient stretching flow. *Phys. Rev. E* **2011**, *84*, 026313.
- (39) Herbst, D. C. Pinch-off of underwater air bubbles with up-down asymmetry. *arXiv:1210.7826*.
- (40) Schwalb, W.; Ng, T. W.; Lye, J. K. K.; Liew, O. W.; Cheong, B. H.-P. Surface tension drawing of liquid from microplate capillary wells. *J. Colloid Interface Sci.* **2012**, *365*, 314–319.
- (41) Gao, L.; McCarthy, T. J. Wetting 101. *Langmuir* **2009**, *25*, 14105–14115.
- (42) Wasan, D. T.; Nikolov, A. D. Spreading of nanofluids on solids. *Nature* **2003**, *423*, 156–159.
- (43) Ng, T. W.; Panduputra, Y. Dynamical force and imaging characterization of superhydrophobic surfaces. *Langmuir* **2012**, *28*, 453–458.
- (44) Paxson, A. T.; Varanasi, K. K. Self-similarity of contact line depinning from textured surfaces. *Nat. Com.* **2013**, *4*, 1492 DOI: 10.1038/ncomms2482.
- (45) Oliver, J. F.; Huh, C.; Mason, S. G. Resistance to spreading of liquids by sharp edges. *J. Colloid Interface Sci.* **1977**, *59*, 568–581.
- (46) Li, X. Y.; Cheong, B. H.-P.; Somers, A.; Liew, O. W.; Ng, T. W. Surface-scribed transparency based microplates. *Langmuir* **2013**, *29*, 849–855.
- (47) Stride, G. O. The respiratory bubble of the aquatic beetle, *Potamodytes tuberosus*, Hinton. *Nature* **1953**, *171*, 885–886.
- (48) Arscott, S. Electrowetting of soap bubbles. *Appl. Phys. Lett.* **2013**, *103*, 014103–014106.